High cholesterol level is essential for myelin membrane growth

Gesine Saher[1], Britta Brügger[2], Corinna Lappe-Siefke[1], Wiebke Möbius[3], Ryu-ichi Tozawa[4], Michael C Wehr[1], Felix Wieland[2], Shun Ishibashi[5] & Klaus-Armin Nave[1,6]

Cholesterol in the mammalian brain is a risk factor for certain neurodegenerative diseases, raising the question of its normal function. In the mature brain, the highest cholesterol content is found in myelin. We therefore created mice that lack the ability to synthesize cholesterol in myelin-forming oligodendrocytes. Mutant oligodendrocytes survived, but CNS myelination was severely perturbed, and mutant mice showed ataxia and tremor. CNS myelination continued at a reduced rate for many months, and during this period, the cholesterol-deficient oligodendrocytes actively enriched cholesterol and assembled myelin with > 70% of the cholesterol content of wild-type myelin. This shows that cholesterol is an indispensable component of myelin membranes and that cholesterol availability in oligodendrocytes is a rate-limiting factor for brain maturation.

During vertebrate brain development, oligodendroglial cells ensheath axonal processes, assemble compact myelin and form the white matter. Myelin provides electrical insulation to the axon and is essential for rapid saltatory impulse conduction. Each myelin sheath represents a spiral extension of the oligodendroglial plasma membrane and appears in cross-sections as a compact, multilayered stack of membranes[1]. In addition to myelin-specific membrane proteins, myelin contains an exceptionally high content of lipids (70% of dry weight). Moreover, more than 25% of the total lipid content is cholesterol, compared to less than 20% in other plasma membranes[2]. Notably, cholesterol is not imported to the brain from the circulation[2].

Based on *in vitro* observations, cholesterol has been implicated in several subcellular functions. It fulfills structural tasks within membranes, such as influencing membrane thickness and fluidity[3], as well as limiting ion leakage through membranes[4], which may be relevant to its property of electrical insulation. Cholesterol, glycosphingolipids and certain membrane proteins can be copurified as detergent-insoluble membrane (DRM) complexes[5]. These complexes have been proposed to correspond to cellular membrane microdomains ('rafts') that serve as platforms for protein sorting[5] and signal transduction[6]. Recently, it has been suggested that myelin membranes may result from the accumulation of myelin-specific rafts in which cholesterol is closely associated with myelin membrane proteins[7,8].

Neither the complete disruption of cholesterol synthesis nor its chemical modulation permits investigation of the role of cholesterol in brain maturation. Previous attempts to study cholesterol function involved chemical extraction[9], a procedure that is not applicable *in vivo*. Chemical inhibitors[10] such as statins modulate cholesterol synthesis but are too nonspecific and toxic when given at concentrations sufficient to shut off cholesterol synthesis[10]. For *in vivo* analysis, we have chosen squalene synthase (SQS; farnesyl-pyrophosphate:farnesyl-pyrophosphate farnesyltransferase, EC 2.5.1.21), which catalyzes the condensation of squalene synthase, the first step specific to sterol biosynthesis[11] (**Fig. 1a**). Complete inactivation of this enzyme, or of 3-hydroxy-3-methylglutaryl coenzyme A (HMG-CoA), the rate-limiting enzyme of this pathway, is lethal during embryonic development[12,13].

Here we describe an essential function of cholesterol in CNS myelination by studying mice with a conditional mutation of the SQS gene (*Fdft1*) in oligodendrocytes. Conditional mutants have severely perturbed myelin synthesis, indicating that oligodendrocytes are the producers of cholesterol in normal brain white matter. However, mutant oligodendrocytes survive by using cholesterol from neighboring wild-type cells of other types. Any myelin made has levels of cholesterol close to normal, thus demonstrating that cholesterol availability is the critical prerequisite and a limiting factor (quantitatively) of myelin membrane growth during brain maturation.

RESULTS

Inactivating SQS function in myelin-forming glial cells

We generated a conditional allele of the *Fdft1* gene in the mouse by introducing two *lox*P sites flanking exon 5 (**Fig. 1b,c**). Exon 5 of *Fdft1* encodes the active site of the enzyme[14]; removal of exons 4 and 5 inactivates SQS function in a conventional *Fdft1* null mutant[13]. Mice with the conditional allele, referred to as SQS-flox mice, developed normally (**Fig. 1d** and data not shown).

[1]Department of Neurogenetics, Max Planck Institute of Experimental Medicine, 37075 Goettingen, Germany. [2]Biochemie-Zentrum, Ruprecht-Karls-Universität Heidelberg, 69120 Heidelberg, Germany. [3]Department of Cell Biology, Universitair Medisch Centrum Utrecht, 3584 CX Utrecht, The Netherlands. [4]Department of Metabolic Diseases, University of Tokyo, Tokyo 113-8655, Japan. [5]Department of Medicine, Jichi Medical School, Tochigi 329-0498, Japan. [6]Hertie Institute of Multiple Sclerosis Research, 37075 Goettingen, Germany. Correspondence should be addressed to K.-A.N. (nave@em.mpg.de).
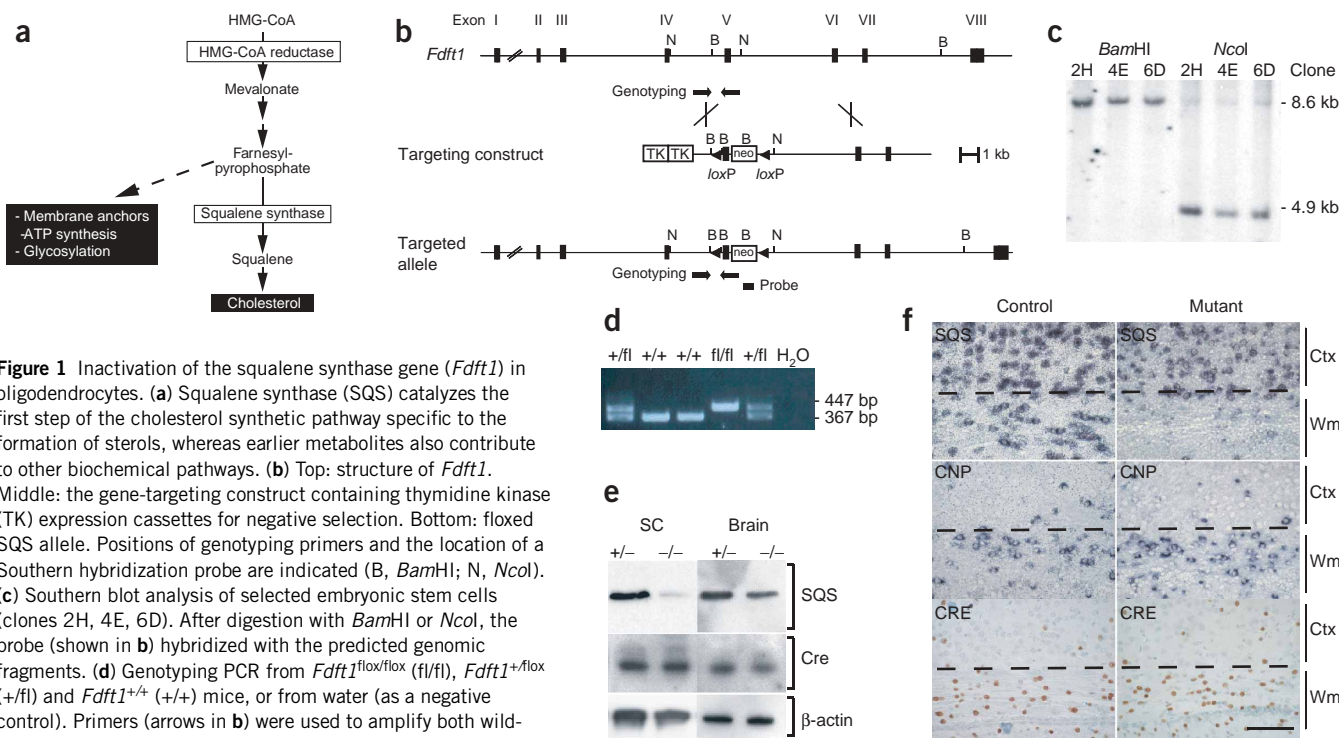
Figure 1 Inactivation of the squalene synthase gene (*Fdft1*) in oligodendrocytes. (**a**) Squalene synthase (SQS) catalyzes the first step of the cholesterol synthetic pathway specific to the formation of sterols, whereas earlier metabolites also contribute to other biochemical pathways. (**b**) Top: structure of *Fdft1*. Middle: the gene-targeting construct containing thymidine kinase (TK) expression cassettes for negative selection. Bottom: floxed SQS allele. Positions of genotyping primers and the location of a Southern hybridization probe are indicated (B, *Bam*HI; N, *Nco*I). (**c**) Southern blot analysis of selected embryonic stem cells (clones 2H, 4E, 6D). After digestion with *Bam*HI or *Nco*I, the probe (shown in **b**) hybridized with the predicted genomic fragments. (**d**) Genotyping PCR from *Fdft1*flox/flox (fl/fl), *Fdft1*+/flox (+/fl) and *Fdft1*+/+ (+/+) mice, or from water (as a negative control). Primers (arrows in **b**) were used to amplify both wild-type (367 bp) and mutant alleles (447 bp). (**e**) Western blot analysis of SQS (48 kDa) and Cre (38 kDa) in total brain and spinal cord lysates, prepared from P20 controls (+/−) and mutants (−/−). Comparable staining of β-actin demonstrates equal loading of protein. (**f**) *In situ* hybridization of cortex (Ctx) and subcortical white matter (Wm) of P17 mice using riboprobes (SQS, top; CNP, middle). Arrowheads point to white matter oligodendrocytes of mutant mice that express CNP but did not express SQS. Labeling of oligodendrocytes for Cre (bottom) confirms that targeted cells are not lost. Scale bar, 50 µm.

To inactivate cholesterol biosynthesis in oligodendrocytes, we crossed SQS-flox mice with mice expressing Cre under the control of the 2′,3′-cyclic nucleotide phosphodiesterase (CNP) promoter (referred to as CNP-Cre mice)[15]. In CNP-Cre mice, Cre expression is restricted almost exclusively to oligodendrocytes and Schwann cells and, like expression of CNP (encoded by the gene *Cnp1*), is first detectable in oligodendrocyte precursor cells[15–17]. In subsequent generations, we obtained mice with the genotype *Fdft1*flox/flox*Cnp1*+/Cre, referred to as 'SQS mutants' or '−/−'. Healthy littermates with the genotype *Fdft1*+/flox*Cnp1*+/Cre are referred to as 'controls', or '+/−'. Both mutants and controls were thus heterozygous for *Cnp1*; control mice developed normally[15].

Mutant mice were born at the expected mendelian ratio and were indistinguishable from controls at birth. To verify the genetic defect, we determined the amount of SQS protein by western blotting of brain and spinal cord lysates at postnatal day 20 (p20) and found a quantitative reduction of SQS in mutants (**Fig. 1e**).

To prove inactivation of *Fdft1* in oligodendrocytes, we assessed the expression of SQS mRNA by *in situ* hybridization using a riboprobe specific for exon 5 of SQS mRNA, to distinguish Cre-recombinant from wild-type cells. In control mice, we detected SQS mRNA in almost all brain regions (**Fig. 1f**, upper left). In contrast, mutant animals largely lacked SQS-specific signals in the white matter, such as the corpus callosum (**Fig. 1f**, upper right). The SQS-deficient cells were oligodendrocytes, as judged by their size and characteristic arrangement in chains. Moreover, *in situ* hybridization of CNP mRNA labeled the same group of cells (**Fig. 1f**, middle) that lacked SQS mRNA. When oligodendrocytes from neonatal mutant mice were maintained in cell culture and immunostained, virtually all CNP-positive cells also were Cre-positive

and showed strongly diminished SQS signals (**Supplementary Fig. 1** online). Thus, all oligodendrocytes showed evidence of Cre-mediated recombination leading to the subsequent loss of SQS expression.

We determined the density of Cre-positive cells in white matter in tissue sections from P20–P100 mice, which showed that mutant oligodendrocytes were present and did not reveal any obvious cell loss (**Fig. 1f**). In the corpus callosum at P20, we counted $3.4 \times 10^3 \pm 0.5 \times 10^3$ cells/mm^2 in mutants, compared to $3.0 \times 10^3 \pm 0.3 \times 10^3$ cells/mm^2 in controls on comparable 4-µm sections. Moreover, western blotting of brain extracts showed an equal steady-state abundance of Cre protein (**Fig. 1e**). With TUNEL staining, we found the same low number of apoptotic cells in the brain (fewer than five cells per coronal section; data not shown), providing independent evidence that oligodendrocyte death was not unusually prevalent.

Ataxia, tremors, and premature death

Despite their identical appearance at birth, mutant mice lagged behind controls in weight gain, and although both sexes were fertile, mutants' overall breeding performance was poor. All mutant mice developed motor function deficits at about 2 weeks of age, coinciding with the known peak of CNS myelination in wild-type mice. The deficits included ataxia, initiation tremor and impaired control of hindlimb movements (**Fig. 2a** and **Supplementary Video 1** online). When quantified by rotarod testing at P20, the motor performance of all mutants was markedly lower than that of controls (**Fig. 2b**).

About one-third of mutant mice died between 20 and 30 d (**Fig. 2c**). Notably, mutants that survived past 1 month of age rarely died prematurely, suggesting that older animals had overcome a critical period in this disorder. The probability of premature death was
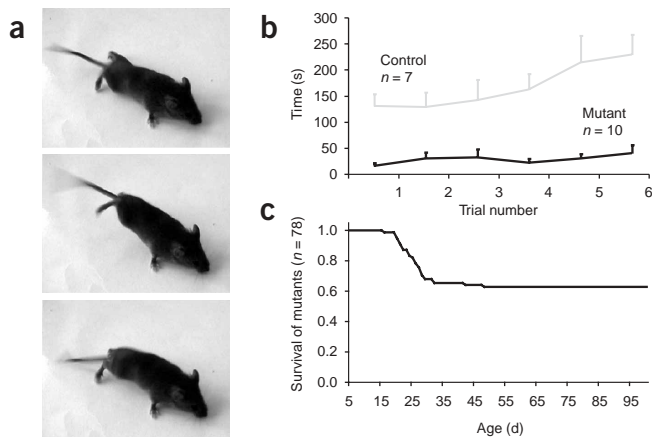
Figure 2 Clinical phenotype. (**a**) Consecutive frames (25 Hz) taken from a video clip of 20-d-old mutant mice, with tremor and ataxia (**Supplementary Video 1**). (**b**) Analysis of motor performance of P20 mice using a standardized accelerating rotarod test with six trials. Mutant mice (black) showed worse motor performance than littermate controls (gray) when total holding time was scored. Values are expressed as mean ± s.e.m. (**c**) Kaplan-Meier survival curve of mutant animals (*n* = 78). About one-third of mutant mice died during the third and fourth weeks; after that point, the clinical phenotype seemed to be stable.

unrelated to the severity of the motor function defect. Premature death may be caused by lethal seizures, although we never observed acute seizures.

Hypomyelination of CNS white matter

On histological sections, we visualized myelin by Gallyas silver impregnation[18] and immunostained for the myelin-specific proteins proteolipid protein (PLP/DM20, encoded by *Plp1*) and CNP. There was a severe dysmyelination of the spinal cord white matter, which was almost devoid of myelin at P20 (**Fig. 3a**). The corpus callosum (**Fig. 3a**) and the cerebellar white matter (data not shown) also showed a marked reduction of myelin

Figure 3 Hypomyelination of CNS white matter tracks. (**a**) Sections of brain and spinal cord of P20 animals were impregnated with silver to visualize myelin (Gallyas) or were immunostained for myelin proteins (PLP and CNP). Arrows point to the corpus callosum (cc), which is hypomyelinated in the mutant brain (ctx, cortex; hc, hippocampus). Dysmyelination of white matter tracts is more obvious in the spinal cord. Boxed areas indicate the position of detailed views shown below (GM, gray matter; WM, white matter; scale bar, 100 μm). (**b**) Ultrastructural analysis of spinal cord at P20. In white matter of control animals (left), virtually all axons (ax) are myelinated, whereas fibers in mutants (right) possess a thin myelin sheath or lack myelin. This dysmyelinating phenotype is less pronounced in gray matter, where axons have myelin of comparable thickness in both control and mutant mice (ax1, unmyelinated axon; ax2, axon with thinner myelin; m, myelin; scale bar, 1 μm).
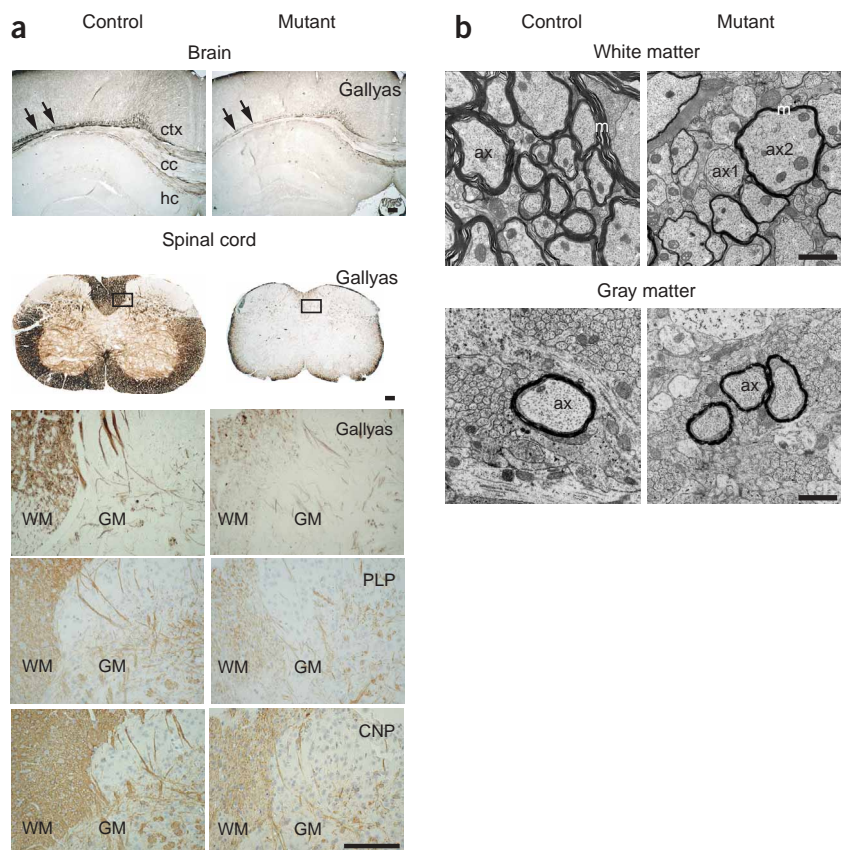
staining in mutant mice. We confirmed the severe dysmyelination of white matter fiber tracts by electron microscopy of lumbar spinal cord (**Fig. 3b**). In mutant mice, most axons showed abnormally thin myelin sheaths or were unmyelinated. In contrast, in gray matter areas such as the central spinal cord, myelin appeared nearly normal and axons showed little difference in myelin thickness (**Fig. 3b**).

To estimate the degree of hypomyelination semiquantitatively, we determined the ratio of myelinated axons in the lateral funiculus of the thoracic spinal cord (*n* = 2 each) at early stages (P9) and during the peak of myelination (P20). In control mice, 58 ± 7% of axons possessed a thin myelin sheath at P9. At P20, virtually all axons (90 ± 2%) were myelinated, and myelin thickness had reached almost adult levels. In contrast, in SQS mutant mice, only a few axons (12 ± 4%) were myelinated at P9, and this fraction increased to only 33 ± 3% at P20. In addition, the myelin thickness in mutant mice never reached control levels (also see below). Thus, myelination was affected early in the assembly process.

Taken together, these results indicate that mutant oligodendrocytes are capable of forming myelinating processes but that myelination is quantitatively impaired. The severity of hypomyelination differs markedly between CNS regions. Although we cannot exclude lineage-related differences between oligodendrocytes of white and gray matter, it is more likely that the ability of oligodendrocytes to make myelin is heavily influenced by neighboring wild-type cells.

The *Cnp1* gene is also expressed in myelin-forming Schwann cells. As expected, SQS mutant mice showed dysmyelination of the peripheral nervous system (data not shown), which is likely to contribute to the described motor defects. However, the clinical phenotype described here is clearly dominated by spinal dysmyelination. A detailed account of the peripheral neuropathy will be reported elsewhere.
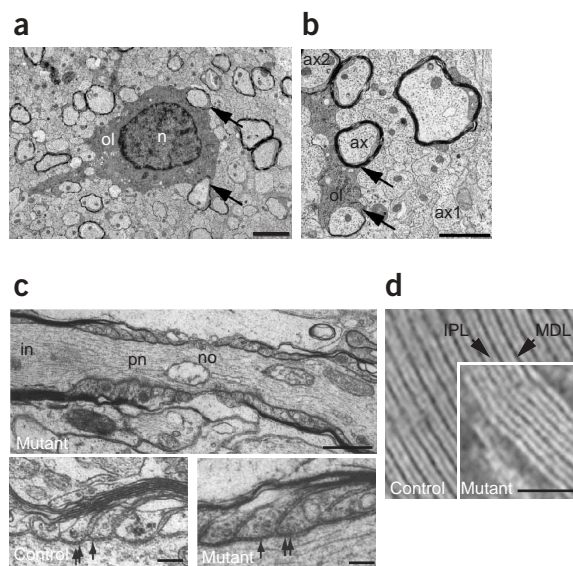
Figure 4 Ultrastructure of oligodendrocytes and myelin. (**a,b**) Ultrastructure of the lumbar spinal cord in mutant mice at P9. Mutant oligodendrocytes (ol) show a normal morphology with dark cytoplasm and processes (marked by arrows) that form a thin myelin sheath around associated axons (ax). n, nucleus. Scale bars: **a**, 2 μm; **b**, 1 μm. (**c**) Ultrastructure of the optic nerve from mutant and control mice at P20. Paranodal structures (pn) are well developed in mutant mice (top). Also at higher magnification, paranodes in control (lower left) and mutant (lower right) mice are indistinguishable including the presence of transverse bands, marked by arrows. in, internode; no, node. Scale bars: 1 μm (top) and 0.2 μm (bottom). (**d**) Ultrastructure of the lumbar spinal cord from mutant and control mice at P20. Compact myelin shows the same periodicity with normal major dense line (MDL) and intraperiod lines (IPL) in mutant (inset at lower right) and control mice. Photomicrographs are aligned to show similarity in periodicity. Scale bar, 50 nm.

Ultrastructure of oligodendrocytes and CNS myelin

All oligodendrocytes appeared morphologically healthy, with dark electron-dense cytoplasm and intact organelle structures. Cell nuclei with clumped chromatin[1] (**Fig. 4a**) did not show signs of degeneration. Likewise, we observed oligodendrocyte processes that connected to myelin sheaths surrounding neighboring axons (arrow in **Fig. 4b**). Thus, when in proximity to wild-type neighboring cells, mutant oligodendrocytes survive, mature and are in a position to ensheath axons for myelin assembly.

A critical structure of myelinated axons is the node of Ranvier[19]. Abnormal nodal regions have been described in mice lacking UDP-galactose:ceramide galactosyltransferase (encoded by *Ugt8*; refs. 20,21). In SQS mutants, however, paranodal loops were indistinguishable from those in wild-type mice, and the nodes were of normal size (**Fig. 4c**). The paranodal regions were narrower, reflecting a reduced number of myelin membrane wraps. We rarely observed abnormal nodal structures, such as outwardly directed paranodal loops, a frequent finding in *Ugt8* null mice[20,21] Also, axonal swellings and axonal degeneration, which are seen in young adult PLP- and CNP-deficient myelin mutants[15,22], were not observed in SQS mutants, even at 6 months of age (data not shown).

Theoretically, reducing cholesterol in oligodendroglial membranes could influence the ultrastructure of myelin and its membrane thickness, periodicity and physical compaction. However, mutant myelin membranes had normal periodicity and a regular compaction, as seen by high-power magnification (**Fig. 4d**). Taken together, these
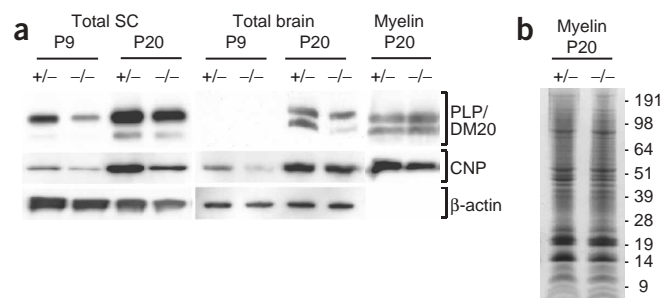
Figure 5 Biochemistry of mutant myelin. (**a**) Western blot comparing the abundance of PLP and CNP in total extracts of spinal cord (Total SC) and brain (Total brain), as well as in purified myelin at the indicated ages. β-actin was used as a loading control. –/–, mutants; +/–, controls. (**b**) Coomassie blue–stained SDS gel (5–12%) of purified myelin membranes of control (+/–) and mutant (–/–) mice. The position of molecular weight marker proteins (in kDa) is indicated.

results indicate that SQS mutant mice have a previously unknown hypomyelinated phenotype but no obvious ultrastructural defects in the myelin architecture.

Myelin protein composition

We found reduced steady-state levels of myelin proteins in brain and spinal cord extracts by western blotting, as shown for PLP and its splice isoform DM20 (PLP/DM20) and CNP (**Fig. 5a**). When equal amounts of purified myelin proteins were stained with Coomassie blue, the overall pattern appeared the same (**Fig. 5b**), and we confirmed this by western blotting to detect individual proteins (**Fig. 5a**). Thus, myelin membranes were less abundant in mutant brains, but they had a normal protein composition.

Cholesterol in myelin

We expected that genetic disruption of cholesterol biosynthesis would alter the lipid composition of oligodendrocytes and, consequently, of myelin. However, a qualitative comparison of mutant and control myelin lipids by thin-layer chromatography (TLC) showed the same pattern for both mutants and controls (**Fig. 6a**). Indeed, cholesterol was present in CNS myelin from mutant mice, indicating that oligodendrocytes had taken up cholesterol for myelin synthesis.

We quantified lipids in purified myelin by nano-ESI-MS/MS mass spectrometry[23] at P20 (**Supplementary Fig. 2** and **Supplementary Table 1** online). When lipid input was normalized to protein content, mass spectrometry showed a 30% reduction in cholesterol in the myelin of mutants (**Fig. 6b**, upper left). Notably, we did not observe a reduction when the cholesterol content was normalized to other membrane lipids, such as phosphatidylcholine (PC) (**Fig. 6b**, upper right). These data point to an unexpected preservation of the cholesterol-to-lipid stoichiometry and imply a reduced overall ratio of lipid to protein in the myelin of SQS mutant mice as compared to controls. Additionally, a direct comparison of the cholesterol levels in total brain with those in purified myelin showed a major 'enrichment' of cholesterol in myelin, both in mutant mice and in controls (**Fig. 6b**, bottom). This strongly suggests that cholesterol incorporation and enrichment is a requirement for myelin membrane growth, independent of the cellular cholesterol source. Taken together, these results show that in mutant myelin, the ratio of cholesterol to protein is reduced. This reduction is not specific for cholesterol, as it affects all major lipids present almost equally, resulting in a preservation of the normal lipid composition of myelin.
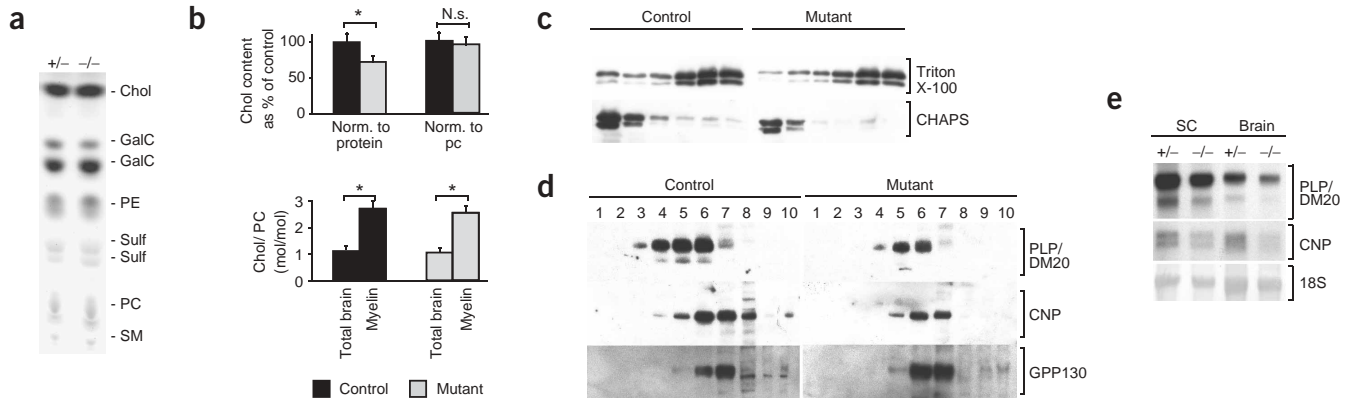
Figure 6 Lipid analysis and detergent-resistant membranes. (**a**) TLC of myelin lipids extracted from purified myelin membranes at P20 (Chol, cholesterol; GalC, galactocerebroside; PE, phosphatidylethanolamin; Sulf, sulfatide; PC, phosphatidylcholine; SM, sphingomyelin). (**b**) Quantitative mass spectrometry of cholesterol and phosphatidylcholine in purified myelin and total brain extracts of P20 animals. Cholesterol content in myelin was normalized to protein input (upper left, mutants: $72.5 \pm 7.8\%$, controls: $100 \pm 11.8\%$) or to phosphatidylcholine (upper right, mutants: $94.9 \pm 10.0\%$). Ratios of cholesterol/ phosphatidylcholine (lower panel) were in determined in myelin (mutants: 2.6 ± 0.26, controls: 2.74 ± 0.31) and total brain extracts (mutants: 1.17 ± 0.15, controls: 1.21 ± 0.12). Values are expressed as mean $\pm$ s.e.m. (*$P < 0.005$; N.s., not significant; $n = 5$–6). (**c**) The presence of PLP/DM20 in DRM from myelin (P20). Numbers indicate density gradient fractions, with fractions 1–2 representing floating proteins, and fractions 5–6 representing soluble proteins. (**d**) Density fractions (1–10) of myelin-free microsomes, prepared from total brain at P20, were assessed for the presence of PLP/DM20 and CNP. The Golgi marker GPP130 served as control. (**e**) Northern blot analysis of PLP/DM20 and CNP expression in spinal cord and brain at P20 (18S ribosomal RNA as loading control).

Myelin proteins in DRM complexes

Cholesterol is an essential component of DRM complexes, hypothesized to form membrane lipid rafts[6] and implicated in myelin biogenesis[9]. Lipid alterations could therefore perturb myelination by limiting protein-lipid interactions. We treated myelin membranes with detergents to assess the presence of DRM and analyzed density gradient fractions by western blot (**Fig. 6c**). As previously reported[9], after Triton X-100 treatment, PLP/DM20 was present predominantly in the soluble fractions, whereas after CHAPS treatment, PLP/DM20 containing DRM floated on top of the gradient. This indicates that in mutants and controls, the interaction of PLP/DM20 and lipids within myelin is very similar.

Excess PLP/DM20 not associating with raft lipids could accumulate in a low-cholesterol subcellular compartment. Such retained protein should be found in higher-density fractions than normally sorted protein. To visualize this 'intracellular pool' of myelin proteins, we prepared myelin-free microsomes from total brain lysates and determined their distribution in a density gradient by western blotting (**Fig. 6d**). We detected PLP/DM20 and CNP in equivalent density fractions in mutant and control animals. Thus, PLP/DM20 and CNP are not missorted within mutant oligodendrocytes. However, the steady-state level of the 'intracellular' PLP/CNP pool was lower in mutant brains than in controls (**Fig. 6d**). This suggests a reduced rate of synthesis of myelin proteins. To determine whether the reduction of cellular myelin proteins could be explained by reduced gene expression, we compared PLP/DM20, CNP and myelin basic protein (MBP) mRNA by northern blot. Transcripts in brain and spinal cord were markedly reduced (**Fig. 6e**, **Supplementary Fig. 3** online and data not shown). Thus, myelin gene expression does not reach its normal peak when cholesterol is limited. This may protect oligodendrocytes from the harmful effects of myelin protein overexpression[22,24,25]. Taken together, these results indicate that cholesterol and myelin lipids associate with PLP in oligodendrocytes, forming DRM complexes ('myelin rafts') with normal biochemical features in mutant mice. However, the reduced availability of cholesterol inhibits high protein expression, possibly at the transcriptional level.

Overcoming dysmyelination by cholesterol uptake

We noticed that the trembling phenotype of mutant mice improved with age. Additionally, silver impregnation of myelin at P100 no longer showed substantial differences between mutant mice and controls (**Fig. 7a**). That was confirmed by western blot analysis: the reduced amounts of myelin proteins seen at P20 were not seen to the same extent at P100 (data not shown). At 3 months, virtually all medium- and large-caliber axons in the spinal cord were myelinated, as shown by electron microscopy, although myelin thickness in the white matter was still below that of controls (**Fig. 7b**).

Astrocytes are a reported source of cholesterol for cultured neurons[26], but whether astrocytes deliver cholesterol *in vivo* to oligodendrocytes is not known. When tissue sections were immunostained for the astroglial marker glial fibrillary acidic protein (GFAP), we observed astrogliosis in mutant spinal cord gray matter at P20 that persisted for at least 6 months (**Fig. 7c**). However, no such astroglial hyperplasia was observed in spinal cord or subcortical white matter. Additionally, immunostaining for macrophage differentiation antigen 3 (MAC-3), a marker of microglia, showed little gliosis (data not shown). Co-staining showed that some GFAP-positive astrocytes in subcortical white matter express HMG CoA reductase, the rate-limiting enzyme of cholesterol synthesis. These astrocytes are in a position to provide cholesterol to mutant oligodendrocytes (**Supplementary Fig. 4** online). The most abundant lipoprotein particles in the CNS contain apolipoprotein E (ApoE), of which astrocytes and microglia are well-known sources[26,27]. In mutants, we found slightly increased steady-state levels of ApoE upon western blotting (**Fig. 7d**), suggestive of enhanced disposal of cholesterol-containing lipoprotein particles. Additionally, low-density lipoprotein receptor related protein (LRP) is one of the major receptors of cholesterol-loaded lipoproteins in the CNS[27]. By western blotting, we found more LRP in the spinal cord of mutant mice than in controls (**Fig. 7d**); it was also expressed in oligodendrocytes, as determined by *in situ* hybridization (data not shown). Thus, LRP is a candidate for cholesterol uptake by mutant oligodendrocytes. These data imply an enhanced horizontal transfer of cholesterol through lipoprotein particles in mutant animals.
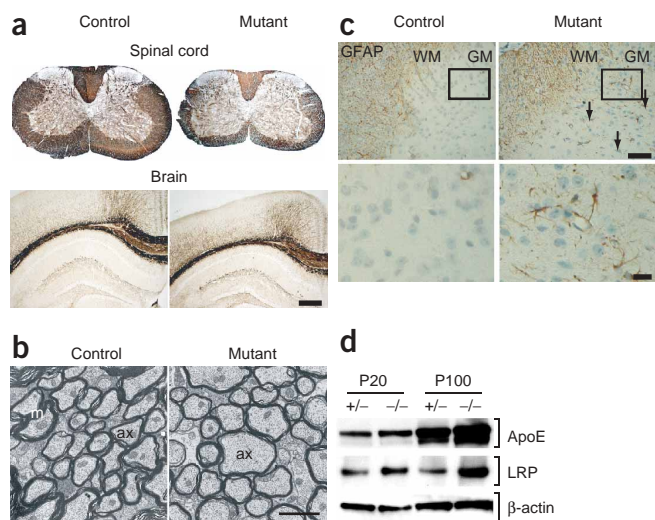
Figure 7 Natural compensation for cholesterol deficiency. (**a**) Histological analysis of adult mice (P100) using Gallyas silver impregnation of myelin (scale bar, 400 μm). (**b**) Ultrastructural analysis of white matter of lumbar spinal cord at P100 confirmed that, as in control animals, all axons (ax) in mutant mice were myelinated (m, myelin). Nevertheless, myelination did not reach control levels (scale bar, 1 μm). (**c**) Astrogliosis in the spinal cord of mutant mice (P20) is shown by an increase in GFAP-positive cells (arrows). Lower panels show an enlarged view of the boxed areas of gray matter (WM, white matter; GM, gray matter; scale bars: upper panel, 50 μm, lower panel, 10 μm). (**d**) Apolipoprotein E (ApoE) and low-density lipoprotein receptor related protein (LRP) were slightly more abundant in mutant (−/−) animals than in control (+/−) animals, as assessed by western blotting in total lysates of spinal cord. β-actin was used as a loading control.

DISCUSSION

We have aimed to elucidate the function of cholesterol in mammalian development *in vivo*. As cholesterol is essential for embryonic development[13], we have developed conditional mouse mutants by Cre-mediated targeting of the *Fdft1* gene. By specifically inactivating *Fdft1* in oligodendrocytes, we were able to observe the first cell type–specific inactivation of cholesterol biosynthesis *in vivo* and describe a previously unknown, informative phenotype. An obvious feature of the conditional mutants is a severely reduced rate of myelination in white matter. This proves unequivocally that the bulk of cholesterol incorporated into myelin is made by oligodendrocytes. The data also demonstrate an efficient horizontal transfer of cholesterol between different brain cell types, which is relevant to neurodegenerative diseases. That mutant oligodendrocytes depend on the local supply of cholesterol is supported by the unexpected finding that purified myelin from mutant mice has an almost normal composition of proteins and lipids, including the characteristic high cholesterol level. Myelin cannot be synthesized without cholesterol, or even with the normal cholesterol content of plasma membranes; only a moderate reduction of the cholesterol-to-protein ratio is tolerated. Thus, the availability of cholesterol is an essential, rate-limiting factor for myelin growth.

Oligodendrocyte survival

The emergence of oligodendrocyte precursors requires the expression of *Olig1* and *Olig2*, which is dependent on sonic hedgehog (Shh)[28]. Theoretically, dysmyelination could result from a defect in cholesterol-dependent Shh signaling and from a diminished number of newly generated oligodendrocytes. This is unlikely, however, because CNP promoter activity begins only in committed oligodendrocyte

precursors, which are Shh independent[29,30]. In fact, pre-existing levels of SQS in newly generated oligodendrocytes may allow for some cholesterol biosynthesis until the onset of myelination.

When cholesterol synthesis is blocked by enzymatic inhibitors, the accumulation of metabolites can be cytotoxic[31,32]. However, we did not find an accumulation of such metabolites by mass spectroscopy (data not shown). Although we cannot formally exclude their abnormal formation, it is more likely that these lipid metabolites do not occur or are efficiently cleared. We occasionally noticed amorphous inclusions in the cytoplasm of some mutant oligodendrocytes by electron microscopy (data not shown). The nature of the aggregates is presently unknown, but they are unlikely to cause the observed phenotype of mutant mice.

Horizontal cholesterol transfer

The net transfer of cholesterol from wild-type cells to SQS-deficient oligodendrocytes is notable, given the extent of myelination in some brain areas. It is likely that some oligodendrocytes (in cortical gray matter, for example) are 'privileged' because of the numerous neighboring wild-type cells, such as astrocytes. We have found increased steady-state levels of ApoE and LRP, suggesting an enhanced lipoprotein particle–mediated cholesterol transfer in mutant mice. Whether levels of these particles are rate limiting for myelination in mutants remains to be determined. Given the overall low level of ApoE and LRP, horizontal cholesterol transfer may also involve other still undefined mechanisms. High dietary cholesterol did not influence the developmental delay of mutant mice (**Supplementary Fig. 5** online), suggesting that bulk transfer of cholesterol from the periphery is not responsible for myelination in mutant mice.

Cholesterol-dependent dysmyelination

The 'checkpoints' at which normal cholesterol levels are required may involve more than one molecular mechanism. Myelin is assembled by vesicular trafficking of membranes that contain myelin-specific proteins, glycolipids and cholesterol[7,8]. A critical stoichiometry of lipid and protein could be controlled within a late Golgi compartment or within a sorting endosome. The association of cholesterol with myelin proteins could stabilize a conformation that is required for further transport to the myelin compartment. We were surprised to find that PLP/DM20 was contained in DRM complexes from SQS mutant mice in equal amounts as in controls (that is, in total brain extracts, purified myelin and brain microsomes). Thus, raft formation in mutant oligodendrocytes is not impaired and PLP/DM20 not missorted.

In mutant oligodendrocytes, the pool of microsomal (that is, cellular) myelin proteins and their corresponding mRNAs did not reach normal peak levels. We hypothesize that oligodendrocytes sense the mismatch in the protein/cholesterol ratio and react by attenuating myelin gene expression accordingly. Normally, the level of cholesterol in membranes is tightly regulated by sterol regulatory element–binding transcription factor 2 (SREBP-2), a cholesterol-regulated transcription factor[33]. In the course of Schwann cell development, SREBP-2 expression is correlated with the concerted expression of myelin lipids[34]. Whether coordinating the ratio of myelin proteins to lipids involves SREBP function needs to be explored. Notably, the transcription of HMG-CoA reductase, a direct SREBP target, is not upregulated in oligodendrocytes (**Supplementary Fig. 4**).

Steroid hormones such as progesterone are made by oligodendrocytes, and progesterone stimulates myelin gene expression[35]. The lack of cholesterol biosynthesis could diminish steroid hormone levels, leading secondarily to hypomyelination, but that seems unlikely.

We found the same level of progesterone in brain lysates from mutants (6.0 ± 0.65 ng per g protein) and controls (6.4 ± 0.6 ng per g protein), suggesting that brain progesterone levels are not limiting.

Comparison with other myelin mutant mice

Hypomyelination is a well-known phenotype of mice with gain-of-function mutations in myelin protein genes[36]. In the complete absence of most myelin proteins, including PLP/DM20, MOG, P0, OSP (claudin-11), MAL and PMP22 (ref. 36), significant myelin assembly is possible. To our knowledge, MBP is the only myelin component beside cholesterol that is required and rate-limiting for myelin membrane growth[25,37].

Previous genetic approaches to study the function of lipids in myelin have involved two myelin-specific glycolipids: galactocerebroside (GalC) and its sulfated derivative[20,21]. Myelination is not prevented in these mutant mice, which have a complex phenotype with signs of dysmyelination and demyelination. Indeed, myelin gene expression remains high in GalC-deficient oligodendrocytes, despite an altered myelin lipid profile[20,21]. An important phenotype of GalC-deficient mice is the instability of paranodal junctions, which reduces the insulating capacity of myelin[20,21], a feature not found in SQS mutant mice.

Implication for human cholesterol deficiency diseases

Several genetic disorders of the cholesterol biosynthetic pathway have been reported in humans. They are associated with myelination defects but also include complex craniofacial malformations[38]. Mouse mutants lacking 7-dehydrocholesterol reductase ($Dhcr7^{-/-}$) are a model for human Smith-Lemli-Opitz-syndrome[31], and mutants lacking 24-dehydrocholesterol reductase ($Dhcr24^{-/-}$) are a model of desmosterolosis[39]. Both genetic disorders affect the last steps of cholesterol biosynthesis, and the phenotypes are also determined by the presence of precursor sterols.

Sterol precursors cannot fully substitute for cholesterol itself and may exert harmful effects[31]. Thus, to understand normal cholesterol biology, it is an advantage that SQS-deficient mutants show no compensation by cholesterol-like precursors. We anticipate that floxed SQS mice, when combined with different patterns of Cre expression in the brain, will allow systematic exploration of the biological function of cholesterol *in vivo*, aspects of horizontal cholesterol transfer and the effect of pharmacological interventions.

METHODS

Molecular cloning. A targeting vector for the mouse *Fdft1* gene was constructed with Sv129 genomic DNA extending from intron 4 to intron 7 and was cloned into a modified pGEM3Zf(+) vector (Promega). One *lox*P site was inserted 5′ to exon 5 using a *Bam*HI site. A neomycin selection cassette and the second *lox*P site were introduced 3′ to exon 5 using an *Eco*RV site.

Mouse genetics. All animal experiments were approved by the state of Niedersachsen, Germany. Positively selected embryonic stem cell clones (E14.1Sv129/OLA, kindly provided by N. Brose, Max Planck Institute of Experimental Medicine, Goettingen, Germany) were identified by PCR. All primer sequences are available upon request. To verify single transgene integration, we performed genomic Southern blotting using a radiolabeled probe of the *neo* resistance gene. C57Bl/6J blastocyst injection was done as previously described[40]. Progeny of a chimera with germline transmission gave rise to the SQS-flox mouse line. For genotyping, genomic DNA was isolated from tail biopsies using the DNeasy 96 tissue kit (Qiagen) and analyzed by PCR. To minimize possible influences of the genetic background, mutants and control littermates were analyzed. Survival curves were calculated according to Kaplan-Meier.

Motor performance assay. Motor coordination and balance were measured by performance on the rotarod[41]. Briefly, after placing mice on a rod, rotation was initiated with increasing speeds from 2–20 rpm in 60 s intervals and latency to fall was recorded (trial completion, 300 s). Values are expressed as mean ± s.e.m.

RNA analysis. For northern blotting, brain RNA purification and hybridization was done as described[15] using radiolabeled probes corresponding to mouse PLP or CNP coding sequences. For *in situ* hybridization, digoxigenin UTP–labeled cRNA probes were generated using a labeling kit (Promega). *In situ* hybridization was performed as described[42].

Antibodies. Antibodies detecting the following proteins were used: SQS (Becton & Dickinson) 1:1,000; CNP (Sigma) 1:300; Cre and GPP130 (Babco) both 1:500; MAG (Chemicon) 1:500 or 1:20 (ref. 43); PLP-A431 (ref. 44) 1:500; Actin (Sigma) 1:1,000; LRP (Transduction Laboratories) 1:200; and GFAP (Chemicon) 1:500.

Protein analysis. For total lysates, whole brains (1:10 wt/vol) were homogenized on ice in lysis buffer (1% Triton X-100, 20 mM Tris-HCl pH 8.0, 137 mM NaCl, 2 mM EDTA, with protease inhibitors (Complete, Roche)). Myelin membranes were purified as described[45]. Detection of immunolabeled protein was performed using chemiluminescence (NEN Life Science Products). Representative results from at least three independent experiments are shown.

Preparation of DRM fractions. DRM assays of purified myelin membranes were performed as described[9,46]. To prepare intracellular membranes, we isolated brain microsomes by differential centrifugation after the removal of myelin membranes[47] and processed them as described[48].

Histology and electron microscopy. On paraffin-embedded tissue sections (4 μm), we visualized myelinated fibers by Gallyas silver impregnation[18]. For immunohistochemistry, we used the Dako-LSAB$_2$ system (Dako), or standard procedures[43] for the analysis of MAG. Sections were analyzed by light microscopy (Zeiss Axiophot). For electron microscopy, we embedded perfused tissue in epoxy resin (Serva) as described[15], before examination (EM912AB, Leo).

Lipid analysis. Total lipid extracts of CNS myelin were made by standard procedures[49], and processed for TLC as described[9]. Progesterone in total brain lysates was measured using the Elecsys progesterone chemiluminescence assay (Roche).

Mass spectrometry. Electrospray ionization (ESI) coupled with collision-induced dissociation (CID) and mass spectrometry (either MS/MS or time-of-flight) was performed as described[23]. Cholesterol was normalized to either protein or phosphatidylcholine contents. Values were expressed as mean percentages of control contents ± s.e.m. Significance was determined using Student's *t*-test of two-tailed uncoupled samples.

Note: Supplementary information is available on the Nature Neuroscience website.

1. Peters, A., Palay, S.L. & Webster, H.D. *The Fine Structure of the Nervous System— the Neurons and Supporting Cells* 3rd edn. (Oxford Univ. Press, New York, 1991).
2. Morell, P. & Jurevics, H. Origin of cholesterol in myelin. *Neurochem. Res.* **21**, 463–470 (1996).
3. Ohvo-Rekila, H., Ramstedt, B., Leppimaki, P. & Slotte, J.P. Cholesterol interactions with phospholipids in membranes. *Prog. Lipid Res.* **41**, 66–97 (2002).
4. Haines, T.H. Do sterols reduce proton and sodium leaks through lipid bilayers? *Prog. Lipid Res.* **40**, 299–324 (2001).

5. Brown, D.A. & London, E. Structure and function of sphingolipid- and cholesterol-rich membrane rafts. *J. Biol. Chem.* **275**, 17221–17224 (2000).
6. Simons, K. & Toomre, D. Lipid rafts and signal transduction. *Nat. Rev. Mol. Cell Biol.* **1**, 31–39 (2000).
7. Kramer, E.M., Schardt, A. & Nave, K.A. Membrane traffic in myelinating oligodendrocytes. *Microsc. Res. Tech.* **52**, 656–671 (2001).
8. Larocca, J.N. & Rodriguez-Gabin, A.G. Myelin biogenesis: vesicle transport in oligodendrocytes. *Neurochem. Res.* **27**, 1313–1329 (2002).
9. Simons, M., Kramer, E.M., Thiele, C., Stoffel, W. & Trotter, J. Assembly of myelin by association of proteolipid protein with cholesterol- and galactosylceramide-rich membrane domains. *J. Cell Biol.* **151**, 143–154 (2000).
10. Michikawa, M. & Yanagisawa, K. Inhibition of cholesterol production but not of nonsterol isoprenoid products induces neuronal cell death. *J. Neurochem.* **72**, 2278–2285 (1999).
11. Bradfute, D.L., Silva, C.J. & Simoni, R.D. Squalene synthase-deficient mutant of Chinese hamster ovary cells. *J. Biol. Chem.* **267**, 18308–18314 (1992).
12. Ohashi, K. *et al.* Early embryonic lethality caused by targeted disruption of the HMG-CoA reductase gene. *J. Biol. Chem.* **278**, 42936–42941 (2003).
13. Tozawa, R. *et al.* Embryonic lethality and defective neural tube closure in mice lacking squalene synthase. *J. Biol. Chem.* **274**, 30843–30848 (1999).
14. Gu, P., Ishii, Y., Spencer, T.A. & Shechter, I. Function-structure studies and identification of three enzyme domains involved in the catalytic activity in rat hepatic squalene synthase. *J. Biol. Chem.* **273**, 12515–12525 (1998).
15. Lappe-Siefke, C. *et al.* Disruption of Cnp1 uncouples oligodendroglial functions in axonal support and myelination. *Nat. Genet.* **33**, 366–374 (2003).
16. Genoud, S. *et al.* Notch1 control of oligodendrocyte differentiation in the spinal cord. *J. Cell Biol.* **158**, 709–718 (2002).
17. Belachew, S., Yuan, X. & Gallo, V. Unraveling oligodendrocyte origin and function by cell-specific transgenesis. *Dev. Neurosci.* **23**, 287–298 (2001).
18. Gallyas, F. Silver staining of myelin by means of physical development. *Neurol. Res.* **1**, 203–209 (1979).
19. Salzer, J.L. Polarized domains of myelinated axons. *Neuron* **40**, 297–318 (2003).
20. Marcus, J. & Popko, B. Galactolipids are molecular determinants of myelin development and axo-glial organization. *Biochim. Biophys. Acta* **1573**, 406–413 (2002).
21. Stoffel, W. & Bosio, A. Myelin glycolipids and their functions. *Curr. Opin. Neurobiol.* **7**, 654–661 (1997).
22. Nave, K.A. & Griffiths, I.R. Models of Pelizaeus-Merzbacher disease. in *Myelin Biology and Disorders* Vol. 2 (ed. Lazzarini, R.A.) 1125–1142 (Academic, London, 2003).
23. Sandhoff, R., Brügger, B., Jeckel, D., Lehmann, W.D. & Wieland, F.T. Determination of cholesterol at the low picomole level by nano-electrospray ionization tandem mass spectrometry. *J. Lipid Res.* **40**, 126–132 (1999).
24. Simons, M. *et al.* Overexpression of the myelin proteolipid protein leads to accumulation of cholesterol and proteolipid protein in endosomes/lysosomes: implications for Pelizaeus-Merzbacher disease. *J. Cell Biol.* **157**, 327–336 (2002).
25. Readhead, C. *et al.* Expression of a myelin basic protein gene in transgenic shiverer mice: correction of the dysmyelinating phenotype. *Cell* **48**, 703–712 (1987).
26. Pfrieger, F.W. Outsourcing in the brain: do neurons depend on cholesterol delivery by astrocytes? *Bioessays* **25**, 72–78 (2003).
27. Herz, J. & Bock, H.H. Lipoprotein receptors in the nervous system. *Annu. Rev. Biochem.* **71**, 405–434 (2002).
28. Lu, Q.R. *et al.* Sonic hedgehog–regulated oligodendrocyte lineage genes encoding bHLH proteins in the mammalian central nervous system. *Neuron* **25**, 317–329 (2000).
29. Alberta, J.A. *et al.* Sonic hedgehog is required during an early phase of oligodendrocyte development in mammalian brain. *Mol. Cell. Neurosci.* **18**, 434–441 (2001).
30. Cooper, M.K. *et al.* A defective response to Hedgehog signaling in disorders of cholesterol biosynthesis. *Nat. Genet.* **33**, 508–513 (2003).
31. Nwokoro, N.A., Wassif, C.A. & Porter, F.D. Genetic disorders of cholesterol biosynthesis in mice and humans. *Mol. Genet. Metab.* **74**, 105–119 (2001).
32. Kim, S.U. Effects of the cholesterol biosynthesis inhibitor ay9944 on organotypic cultures of mouse spinal cord. Retarded myelinogenesis and induction of cytoplasmic inclusions. *Lab. Invest.* **32**, 720–728 (1975).
33. Brown, M.S. & Goldstein, J.L. A proteolytic pathway that controls the cholesterol content of membranes, cells, and blood. *Proc. Natl. Acad. Sci. USA* **96**, 11041–11048 (1999).
34. Verheijen, M.H., Chrast, R., Burrola, P. & Lemke, G. Local regulation of fat metabolism in peripheral nerves. *Genes Dev.* **17**, 2450–2464 (2003).
35. Sereda, M.W., Meyer Zu, H.G., Suter, U., Uzma, N. & Nave, K.A. Therapeutic administration of progesterone antagonist in a model of Charcot-Marie-Tooth disease (CMT-1A). *Nat. Med.* **9**, 1533–1537 (2003).
36. Lazzarini, R.A. *Myelin Biology and Disorders* (Academic, London, 2003).
37. Popko, B. *et al.* Myelin deficient mice: expression of myelin basic protein and generation of mice with varying levels of myelin. *Cell* **48**, 713–721 (1987).
38. Bjorkhem, I. & Meaney, S. Brain cholesterol: long secret life behind a barrier. *Arterioscler. Thromb. Vasc. Biol.* **24**, 806–815 (2004).
39. Wechsler, A. *et al.* Generation of viable cholesterol-free mice. *Science* **302**, 2087 (2003).
40. Joyner, A.L. Gene targeting and gene trap screens using embryonic stem cells: new approaches to mammalian development. *Bioessays* **13**, 649–656 (1991).
41. Jones, B.J. & Roberts, D.J. A rotarod suitable for quantitative measurements of motor incoordination in naive mice. *Naunyn Schmiedebergs Arch. Exp. Pathol. Pharmakol.* **259**, 211 (1968).
42. Schaeren-Wiemers, N. & Gerfin-Moser, A. A single protocol to detect transcripts of various types and expression levels in neural tissue and cultured cells: *in situ* hybridization using digoxigenin-labelled cRNA probes. *Histochemistry* **100**, 431–440 (1993).
43. Huber, A.B., Weinmann, O., Brosamle, C., Oertle, T. & Schwab, M.E. Patterns of Nogo mRNA and protein expression in the developing and adult rat and after CNS lesions. *J. Neurosci.* **22**, 3553–3567 (2002).
44. Jung, M., Sommer, I., Schachner, M. & Nave, K.A. Monoclonal antibody O10 defines a conformationally sensitive cell-surface epitope of proteolipid protein (PLP): evidence that PLP misfolding underlies dysmyelination in mutant mice. *J. Neurosci.* **16**, 7920–7929 (1996).
45. Norton, W.T. & Poduslo, S.E. Myelination in rat brain: method of myelin isolation. *J. Neurochem.* **21**, 749–757 (1973).
46. Brown, D.A. & Rose, J.K. Sorting of GPI-anchored proteins to glycolipid-enriched membrane subdomains during transport to the apical cell surface. *Cell* **68**, 533–544 (1992).
47. Jurevics, H. *et al.* Normal metabolism but different physical properties of myelin from mice deficient in proteolipid protein. *J. Neurosci. Res.* **71**, 826–834 (2003).
48. Plonne, D. *et al.* Separation of the intracellular secretory compartment of rat liver and isolated rat hepatocytes in a single step using self-generating gradients of iodixanol. *Anal. Biochem.* **276**, 88–96 (1999).
49. Bligh, E.G. & Dyer, W.J. A rapid method of total lipid extraction and purification. *Can. J. Med. Sci.* **37**, 911–917 (1959).